





Defect-mediated metastability and carrier lifetimes in polycrystalline (Ag,Cu)(In,Ga)Se₂ absorber materials

Cite as: J. Appl. Phys. **127**, 215702 (2020); <https://doi.org/10.1063/1.5134502>

Submitted: 31 October 2019 . Accepted: 11 May 2020 . Published Online: 02 June 2020

Andrew J. Ferguson , Rouin Farshchi, Pran K. Paul, Pat Dippo, Jeff Bailey, Dmitry Poplavskyy, Afrina Khanam , Filip Tuomisto , Aaron R. Arehart , and Darius Kuciauskas 

COLLECTIONS

Paper published as part of the special topic on [Defects in Semiconductors 2020](#)

Note: This paper is part of the Special Topic on Defects in Semiconductors 2020.

 This paper was selected as an Editor's Pick



View Online



Export Citation



CrossMark

ARTICLES YOU MAY BE INTERESTED IN

[High electron density \$\beta\$ -\(Al_{0.17}Ga_{0.83}\)₂O₃/Ga₂O₃ modulation doping using an ultra-thin \(1nm\) spacer layer](#)

Journal of Applied Physics **127**, 215706 (2020); <https://doi.org/10.1063/5.0005531>

[Texture evolution in nanocrystalline Cu under shock compression](#)

Journal of Applied Physics **127**, 215106 (2020); <https://doi.org/10.1063/5.0006713>

[A low-current atmospheric pressure discharge generating atomic magnesium fluxes](#)

Journal of Applied Physics **127**, 213303 (2020); <https://doi.org/10.1063/5.0006239>

Lock-in Amplifiers
up to 600 MHz



Defect-mediated metastability and carrier lifetimes in polycrystalline (Ag,Cu)(In,Ga)Se₂ absorber materials

Cite as: J. Appl. Phys. **127**, 215702 (2020); doi: [10.1063/1.5134502](https://doi.org/10.1063/1.5134502)

Submitted: 31 October 2019 · Accepted: 11 May 2020 ·

Published Online: 2 June 2020



Andrew J. Ferguson,^{1,a)}  Rouin Farshchi,^{2,a)}  Pran K. Paul,³ Pat Dippo,¹ Jeff Bailey,² Dmitry Poplavsky,² Afrina Khanam,⁴  Filip Tuomisto,^{4,5}  Aaron R. Arehart,³  and Darius Kuciauskas^{1,a)} 

AFFILIATIONS

¹Chemistry & Nanoscience Center, National Renewable Energy Laboratory, 15013 Denver West Parkway, Golden, Colorado 80401, USA

²MiaSolé Hi-Tech Corp., Santa Clara, California 95051, USA

³The Department of Electrical and Computer Engineering, The Ohio State University, Columbus, Ohio 43210 USA

⁴Department of Applied Physics, Aalto University, P.O. Box 15100, FI-00076 Aalto, Finland

⁵Department of Physics and Helsinki Institute of Physics, University of Helsinki, P.O. Box 43, FI-00014 Helsinki, Finland

Note: This paper is part of the Special Topic on Defects in Semiconductors 2020.

a) Authors to whom correspondence should be addressed: andrew.ferguson@nrel.gov; rouin.farshchi@gmail.com; and darius.kuciauskas@nrel.gov

ABSTRACT

Using a combination of optical and electrical measurements, we develop a model for metastable defects in Ag-alloyed Cu(In,Ga)Se₂, one of the leading thin film photovoltaic materials. By controlling the pre-selenization conditions of the back contact prior to the growth of polycrystalline (Ag,Cu)(In,Ga)Se₂ absorbers and subsequently exposing them to various stresses (light soaking and dark-heat), we explore the nature and role of metastable defects on the electro-optical and photovoltaic performance of high-efficiency solar cell materials and devices. Positron annihilation spectroscopy indicates that dark-heat exposure results in an increase in the concentration of the selenium-copper divacancy complex ($V_{\text{Se}}-V_{\text{Cu}}$), attributed to depassivation of donor defects. Deep-level optical spectroscopy finds a corresponding increase of a defect at $E_v + 0.98$ eV, and deep-level transient spectroscopy suggests that this increase is accompanied by a decrease in the concentration of mid-bandgap recombination centers. Time-resolved photoluminescence excitation spectroscopy data are consistent with the presence of the $V_{\text{Se}}-V_{\text{Cu}}$ divacancy complex, which may act as a shallow trap for the minority carriers. Light-soaking experiments are consistent with the $V_{\text{Se}}-V_{\text{Cu}}$ optical cycle proposed by Lany and Zunger, resulting in the conversion of shallow traps into recombination states that limit the effective minority carrier recombination time (and the associated carrier diffusion length) and an increase in the doping density that limits carrier extraction in photovoltaic devices.

Published under license by AIP Publishing. <https://doi.org/10.1063/1.5134502>

I. INTRODUCTION

Thin-film photovoltaic (PV) cells based on the multinary chalcopyrite semiconductors—e.g., Cu(In,Ga)Se₂, CIGS—have achieved power conversion efficiencies (PCEs) exceeding 23% (cell) and 17% (module),¹ and there is significant effort focused at both improving the device performance and addressing stress-induced changes in material properties (metastability) that limit device reliability. One approach that has recently demonstrated promise is the partial

substitution of Ag for Cu, to form pentenary (Ag,Cu)(In,Ga)Se₂ (ACIGS) alloys, where the thin film alloy appears to exhibit good miscibility, particularly, in compositions with less than 50% Ag substitution.² Ag substitution lowers the melting temperature of the multinary chalcopyrite alloys relative to their Cu analogs,³ resulting in reduced disorder (lattice defects) in as-deposited absorber materials.⁴ Depending on the precise absorber composition and processing conditions, PV devices based on ACIGS have yielded improved

PCE, primarily due to an increase in the open-circuit voltage of the device.⁵ This approach has resulted in 20.56% efficient solar cells⁶ and (world record) 18.64% efficient ACIGS modules.^{1,7}

While the precise chemical nature and electronic properties of defects in CIGS semiconductors are a matter of debate,^{8,9} their influence on the performance and metastability of photovoltaic devices is generally accepted,^{10,11} and they are widely explored both theoretically and experimentally. In particular, the selenium-copper divacancy complex ($V_{\text{Se}}-V_{\text{Cu}}$) has been hypothesized to play a major role in the electronic properties of the absorber layer, where according to Lany and Zunger, this defect complex is predicted to change charge state upon light-soaking from a shallow donor to a shallow acceptor accompanied by a deep acceptor level of ~ 1 eV above the valence band.¹⁰ However, to our knowledge, there have been fewer experimental studies linking the electronic properties of ACIGS with defect-induced metastability.¹²

Here, we probe the influence of environmental stress (dark-heat exposure at 85 °C for 1000 h and/or light-soaking under simulated 1 sun AM1.5G illumination for 24 h) on the device performance and charge carrier dynamics in pentenary ACIGS absorbers. Through control of the selenization conditions prior to absorber growth and the application of a suite of experimental techniques, we correlate the observed changes to the ACIGS trap/defect properties. We show that dark-heat exposure increases the concentration of $V_{\text{Se}}-V_{\text{Cu}}$ divacancies in the absorber layer, and that for large concentrations of this defect, subsequent light-soaking can have a detrimental effect on device performance, presumably originating from the light-induced metastability of this defect. We show that the dark heat and light soak induced changes in device performance are sensitive to the degree of selenization of the back-electrode layer prior to absorber growth, consistent with attribution of defect-mediated metastable material properties to selenium vacancy-related defects. We employ positron annihilation spectroscopy (PAS) to identify the $V_{\text{Se}}-V_{\text{Cu}}$ divacancy complex as the dominant annihilation site in the absorber layer, and to reveal increasing levels of this defect complex with dark-heat exposure. We employ sub-bandgap time-resolved photoluminescence (TRPL) excitation and deep level optical spectroscopy (DLOS) to identify defect states located close to the conduction band edge, presumably associated with the $V_{\text{Se}}-V_{\text{Cu}}$ divacancy defect. The density of these states is increased by dark-heat exposure, whereas light soaking results in their conversion to photoluminescence lifetime-limiting recombination centers.

II. EXPERIMENTAL METHODS

A. Solar cell fabrication and stressing

Samples for analysis were prepared from full stack ACIGS solar cells deposited by physical vapor deposition (PVD) in a MiaSolé production roll-coater tool, where all films are deposited sequentially on stainless steel foil in a series of interconnected vacuum chambers.^{13,14} The Mo back electrode was selenized in the PVD chamber prior to the deposition of the absorber layer at either the same level as during growth of the nucleation layer, referred to hereafter as “high Se” or at roughly 12% of that level, referred to as “low Se.” The ACIGS samples under investigation here include both Na and K, which are introduced via diffusion

from the Mo back electrode. The absorber layer ($\sim 1.2 \mu\text{m}$) is sequentially covered with a CdS buffer layer (~ 30 nm), a thin intrinsic ZnO layer (~ 100 nm), and a conductive ZnO layer (300–400 nm), forming the transparent conducting oxide (TCO). For solar cell fabrication, the full stack material from the roll-coater is cut and slit into cells (136.5 cm^2 area), which are finished with a metal grid electrode attached to the top of the TCO layer. For capacitance devices, circular Ni/Al top contacts were deposited via e-beam evaporation on top of the TCO layer, followed by device isolation via scribing a 2 mm^2 circle around the top contacts.

The solar cells, capacitance devices, and full stack samples were encapsulated either between a backsheet and a transparent front barrier or between two transparent barrier layers for protection against moisture ingress during applied stresses. Light-soaking (denoted LS24) was carried out under simulated 1 sun irradiation and open circuit conditions for 24 h, with the module temperature controlled at 55 ± 5 °C. Dark-heat (DH) exposure was carried out at 85 °C for a duration of 1000 h (denoted DH1000). The following stresses were applied sequentially: LS24, DH1000, LS24, where the final light-soaked state will be denoted DH1000 + LS. Prior to PL and PAS measurements, the samples were removed from the packaging, and the TCO window and CdS buffer layers were etched to expose the ACIGS surface.

B. Solar cell characterization

Light I–V measurements on the solar cells were carried out at room temperature under simulated 1 sun illumination using 4-point probe measurements to extract open circuit voltage (V_{oc}), short-circuit current density (J_{sc}), fill factor (FF), and power conversion efficiency. External quantum efficiency (EQE) measurements were carried out on the solar cells at room temperature under zero applied bias using a monochromator over the range of 400–1200 nm. Capacitance–voltage (CV) profiles were measured using a Sula Technologies deep level transient spectroscopy (DLTS) instrument at room temperature over a range from -1.8 V to $+0.5$ V (completed within 1 ms) at 1 MHz and were converted to doping density depth profiles using the Mott–Schottky equation.¹⁵

C. Deep level transient and deep level optical spectroscopy

Fully digital capacitance-based deep level transient spectroscopy (DLTS) and deep level optical spectroscopy (DLOS) measurements were employed to characterize trap states in the ACIGS absorber layer. Combined, DLTS and DLOS allow traps throughout the ACIGS bandgap to be characterized. The DLTS system consists of a LakeShore TTP4 probe station, Boonton 7200 capacitance meter, Agilent 33220A function generator, National Instruments data acquisition system, and custom software. For DLOS, a Quartz Tungsten Halogen (QTH) lamp and monochromator are used to illuminate the sample with monochromatic light. For DLTS, a 0.2 V was applied during the 10 ms fill pulse and -1.0 V applied during the transient measurement. For DLOS, a 0 V fill pulse for 10 s and -1.0 V measurement pulse were applied. Full details of the equipment, techniques, and analysis procedures can be found in Refs. 15–18.

The trap densities, N_{trap} , probed by DLTS and DLOS were calculated using

$$N_{\text{trap}} = 2N_A \cdot \frac{\Delta C}{C_0} \cdot F_{\text{corr}}, \quad (1)$$

where N_A is the doping density at the measurement bias, ΔC is the change in capacitance at the applied voltage, and C_0 is the steady-state capacitance at the measurement bias and temperature of the peak. F_{corr} is a correction factor based on the rate window times (i.e., the rate window only sees a fraction of the total change in capacitance of the entire transient), where $F_{\text{corr}} = 3.07$ for the DLTS and $F_{\text{corr}} = 1$ for DLOS. Additionally, the “lambda correction” (a factor of ca. 3–4 \times) is also applied for the DLTS data and is described in more detail in Ref. 15. This accounts for the fact that traps are not modulated in the entire depletion region but only in the volume where the traps are below the Fermi level in the fill bias and above the Fermi level in the measurement bias. The DLOS trap (ca. 1 eV) does not modulate during the DLTS experiment and the DLTS trap (ca. 0.6 eV) is fully emitted before the DLOS trap was measured by waiting in the dark for several seconds to allow the DLTS trap to emit.

D. Positron annihilation spectroscopy

Doppler broadening measurements of positron annihilation radiation were performed with a variable-energy positron beam. The positron implantation energy was varied between 5 and 25 keV, allowing depths of 0.1–1.2 μm of the absorber layers to be probed. A high purity germanium (HPGe) detector with an energy resolution of 1.2 keV at 511 keV was employed for determining the energies of the annihilation photons. The integration windows for the conventional S and W parameters were set to $|p_L| < 0.4$ a.u. and 1.6 a.u. $< |p_L| < 4.0$ a.u., respectively.¹⁹ The full stack solar cell samples were etched down to the absorber layer with HCl prior to this measurement (TCO and CdS layers removed).

E. Steady-state optical spectroscopy

Excitation was provided by a 632.8 nm HeNe continuous wave laser at varying powers. Emission spectra were collected with a 500 μs exposure time using a Newport MS260i spectrometer, equipped with a 200 grooves/mm grating blazed at 1000 nm, and an InGaAs photodiode array (Princeton Instruments PyLoN-IR).

F. Time-resolved optical spectroscopy

Excitation was provided by an optical parametric amplifier pumped by a Yb:KGW laser with 1.1-MHz repetition rate and pulse length of ca. 0.3 ps (Orpheus/Pharos, Light Conversion). A multi-mode optical fiber was used to guide the excitation beam to the sample. The light was focused at the sample with an aspheric lens (New Focus 5724, numerical aperture NA 0.50), and the excitation spot diameter was approximately 200 μm . The same lens/fiber combination was used to collect the PL signal, which was routed to the detector using a dichroic beam splitter. The TRPL decays were recorded via time-correlated single-photon counting (PicoHarp 300 TCSPC Module, PicoQuant) using a silicon single-photon avalanche diode (Micro Photon Devices).

III. RESULTS AND DISCUSSION

In order to elucidate the role of selenium vacancy-related defects on the material properties of the ACIGS absorbers, we prepared samples with low and high pre-selenization conditions. The level of selenization of the Mo back electrode can potentially impact various critical aspects related to the absorber composition within the solar cell, including (i) Se diffusion into the absorber layer and consequential impact on the formation of defects related to selenium vacancies (e.g., V_{Se} or $V_{\text{Se}}-V_{\text{Cu}}$), grain boundary properties, and stoichiometry of the absorber layer during various stages of high temperature growth, and (ii) diffusion of the Na and K alkali species, which are introduced into the absorber via out-diffusion from the back electrode, and can interact with Se to form sodium or potassium compounds with selenium, as evidenced in secondary phases observed by electron dispersive x-ray spectroscopy in a scanning electron microscope (SEM-EDS),²⁰ in addition to their potential role in passivation of V_{Se} or $V_{\text{Se}}-V_{\text{Cu}}$ defects.

Figures S1 and S2 (supplementary material) illustrate that the selenization level applied to the back electrode prior to growth of the absorber has little impact on the electronic bandgap ($E_g \approx 1.21$ eV) of the ACIGS absorber, which differs by only a few meV. The shape and position of the room-temperature steady-state photoluminescence (PL) spectra, after excitation at 632.8 nm, of the two materials is near identical.

A. Influence of environmental stress on ACIGS device performance

Figure 1 shows light J–V parametrics for the high Se and low Se samples at various stress states. It can be seen that dark heat stress leads to a stronger reduction in open-circuit voltage, V_{oc} , for the high Se sample. This could be at least in part due to the stronger reduction in doping with dark heat for the high Se condition compared to low Se (cf. Fig. 2, *vide infra*). With subsequent light-soaking after DH, namely, DH1000 + LS24, V_{oc} at least partially recovers for both pre-selenization conditions, where this recovery is associated with increased doping concentrations to near LS24 levels. The fill-factor, FF, loss with dark heat is significant for both low and high Se conditions. Current density–voltage–temperature (JVT) measurements previously published for samples similar to those studied here allow us to ascribe the FF losses with DH to an increase of the in-stack barrier height (activation energy) potentially resulting from a reverse-diode located either at the back electrode or the CIGS/buffer interface.²¹ The observed FF loss is partially reversible with a second LS24 treatment, consistent with observed recovery of JVT characteristics. Finally, the short-circuit current density, J_{sc} , is reduced for LS24 samples, most strikingly after DH1000 + LS24 for the low Se condition. We hypothesize that the DH1000 treatment results in an increase in the concentration of $V_{\text{Se}}-V_{\text{Cu}}$ divacancy defects (*vide infra*), and attribute the reduced J_{sc} after the light-soak to conversion of these defects into shallow acceptors and deep Shockley–Read–Hall (SRH) recombination centers, due to the optical cycle proposed by Lany and Zunger. Since the concentration of $V_{\text{Se}}-V_{\text{Cu}}$ divacancy defects is larger for the low Se sample after the DH1000 treatment than the high Se sample, the subsequent light soak results in a larger decrease in the measured J_{sc} .

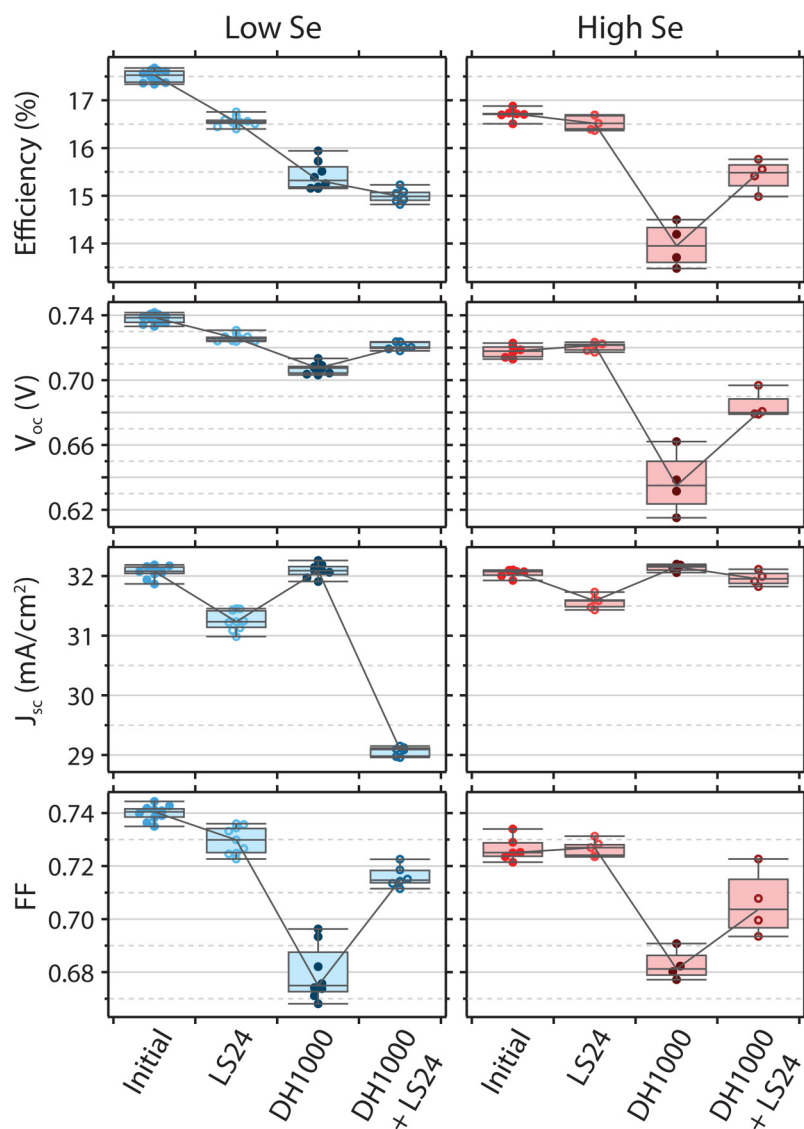


FIG. 1. The impact of light soaking (LS24) and dark-heat exposure (DH1000) on the J-V parametrics extracted from current-voltage measurements for solar cells processed with low (left) and high (right) pre-selenization conditions.

Consistent with previous observations for CIGS devices,²² light soaking results in a reduction in the collection efficiency of the ACIGS devices, as shown in Fig. S2 (supplementary material). This is particularly evident for the low Se sample. In contrast, dark-heat exposure DH1000 seems to recover the spectral response of the initial (as-deposited) devices. However, the low Se sample shows an even larger reduction in collection efficiency after subsequent light-soaking of the DH1000 state (referred to as DH1000 + LS24).

Some observations regarding the effects of environmental stress can be made from fast capacitance-voltage (C-V),²³ which provides information concerning the carrier doping density/profile and depletion width in the ACIGS absorber layer. Figures 2(a) and 2(b) illustrate that dark-heat exposure results in a reduction in the carrier density and an increase in the depletion width, whereas

light soaking causes an order of magnitude increase in the carrier density, with an associated decrease in the depletion width, particularly for the low Se sample. The strong light soaking-induced increase in doping density for the low Se sample and the associated reduction in depletion width is the likely cause for the observed reduction in the collection efficiency and J_{sc} , which is more severe after DH1000. In the following, we aim to understand the reasons for these light-soak induced changes by investigating the nature and role of metastable defects in the absorber layer.

B. Defects in ACIGS absorbers

In order to gain a better understanding of semiconductor defects and the role they play in determining the electro-optical

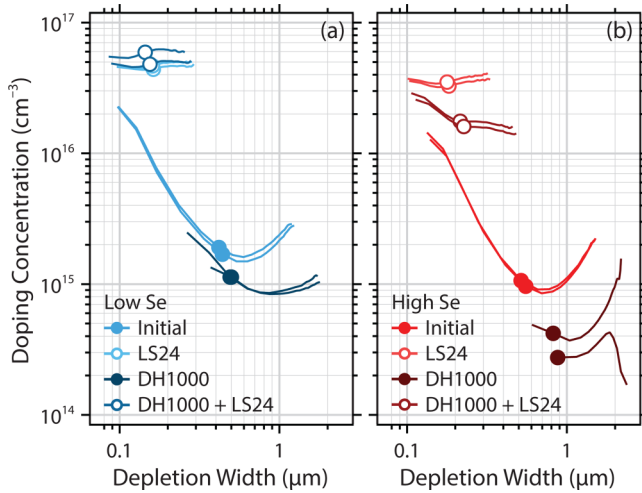


FIG. 2. The impact of light soaking (LS24) and dark-heat exposure (DH1000) on the doping profile of ACIGS samples for (a) low and (b) high pre-selenization conditions. The symbols in (a) and (b) indicate the apparent carrier density and depletion width at zero bias.

properties of ACIGS absorbers, a number of experimental techniques were employed.

Deep level transient spectroscopy (DLTS) measurements on the low selenization sample before and after DH1000 exposure help understand the effect of dark heat on the concentration of deep traps. Figure 3(a) shows the DLTS spectra of the initial and DH1000 samples. Both samples contain $E_V + 0.59$ eV near-mid-gap

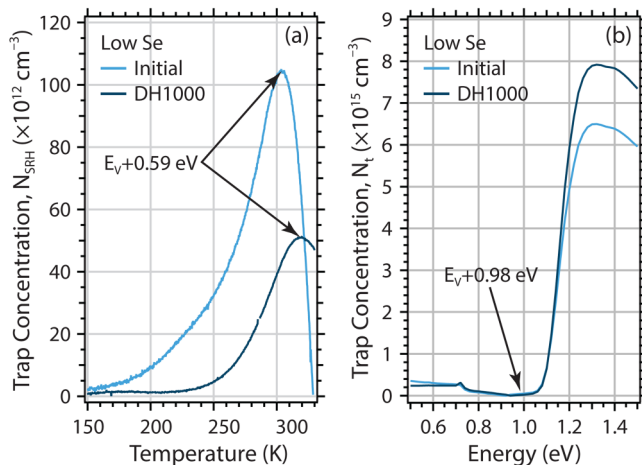


FIG. 3. The impact of dark-heat exposure (DH1000) on the (a) DLTS spectra of the 80 s^{-1} rate window and (b) room temperature DLOS spectra for the ACIGS sample with low selenization. The trap concentration is identified by the peak height and trap energy is calculated by the onset of the steady-state DLOS signal.

traps previously attributed to the Cu_M ($M = \text{Ga}$ or In) antisite defect,²⁴ which are likely Shockley–Read–Hall (SRH) recombination centers.²⁵ The concentration of $E_V + 0.59$ eV traps probed by DLTS is decreased by ca. $2\times$ after DH1000 treatment from $1 \times 10^{14} \text{ cm}^{-3}$ to $5 \times 10^{13} \text{ cm}^{-3}$. The lowering of the midgap trap concentration upon annealing is consistent with the increase in measured lifetime by TRPL after dark heat exposure (*vide infra*) and is likely associated with reduced atomic disorder from annealing, leading to a reduction of Cu_M ($M = \text{Ga}$ or In) substitutional defects.²⁶ The observed reduction in V_{oc} with DH1000, which we attribute to a decrease in carrier concentration, occurs despite this reduction in midgap defects.

To characterize the traps located in the upper half of the bandgap, deep level optical spectroscopy (DLOS) measurements were employed. Figure 3(b) shows the DLOS spectra of low Se samples before and after dark heat exposure. DLOS spectra show an onset at $E_V + 0.98$ eV, which is typically observed for CIGS¹⁷ and is consistent with the observed broad defect excitation band measured using TRPL (Fig. 5). The concentration of the $E_V + 0.98$ eV trap measured by DLOS increased by ca. $1.5 \times 10^{15} \text{ cm}^{-3}$ after DH1000, consistent with the observed increase in PL intensity of the broad absorption between 0.85 and 1.08 eV (Fig. 5).

Positron annihilation spectroscopy is a versatile tool for studying vacancy-type defects in semiconductors, with selective sensitivity to neutral and negatively charged centers. The Doppler broadened spectrum of the positron-electron annihilation radiation peak is analyzed in terms of S and W parameters.^{27,28} The S parameter is the fraction of counts in the central region of the annihilation peak and depends predominantly on the open volume of the vacancy.^{19,28} The W parameter is the fraction of counts in the wing areas on both sides of the peak, which depends on the open volume of the defect and on the chemical nature of the surrounding atoms.^{19,28} The S parameter is associated with the vacancy concentration, while the ratios of the S and W parameters for the vacancy defect with respect to the bulk crystal, commonly referred to as $R = \Delta S / \Delta W$, or the defect specific parameter, indicates the nature of the defect.^{19,28} Here, ΔS and ΔW are defined as changes from annihilation in a localized state in a vacancy defect (S_v, W_v) compared to annihilation in the delocalized state (called bulk) in the lattice (S_b, W_b), namely, $R = |(S_v - S_b) / (W_v - W_b)|$. By analyzing the S and W parameters at different positron implantation energies, the vacancy defect depth profiles can be obtained, and their concentrations determined when in the range of $1 \times 10^{15} - 1 \times 10^{19} \text{ cm}^{-3}$. In this study, the implantation energy was varied from 5 to 25 keV, which roughly corresponds to mean implantation depths in the range of 0.1–1.2 μm . For further details of the method and analysis approaches, see Ref. 19.

Previous positron annihilation studies have identified $V_{\text{Se}} - V_{\text{Cu}}$ divacancies as the dominant positron traps in CIGS absorber materials and have identified the fingerprints for these defect species.²⁸ The data presented in this work are analyzed according to the findings in Ref. 28. The S – W plot for the high and low pre-selenization samples in the initial and DH1000 states is shown in Fig. 4(a). A data point is shown for bulk CIGS, which is the weighted average of (S, W) values measured in CIS and CGS bulk crystals grown by the Bridgman method, described in detail in Ref. 28, weighted according to the stoichiometry $\text{CuIn}_{1-x}\text{Ga}_x\text{Se}$ with $x = 0.4$ for the

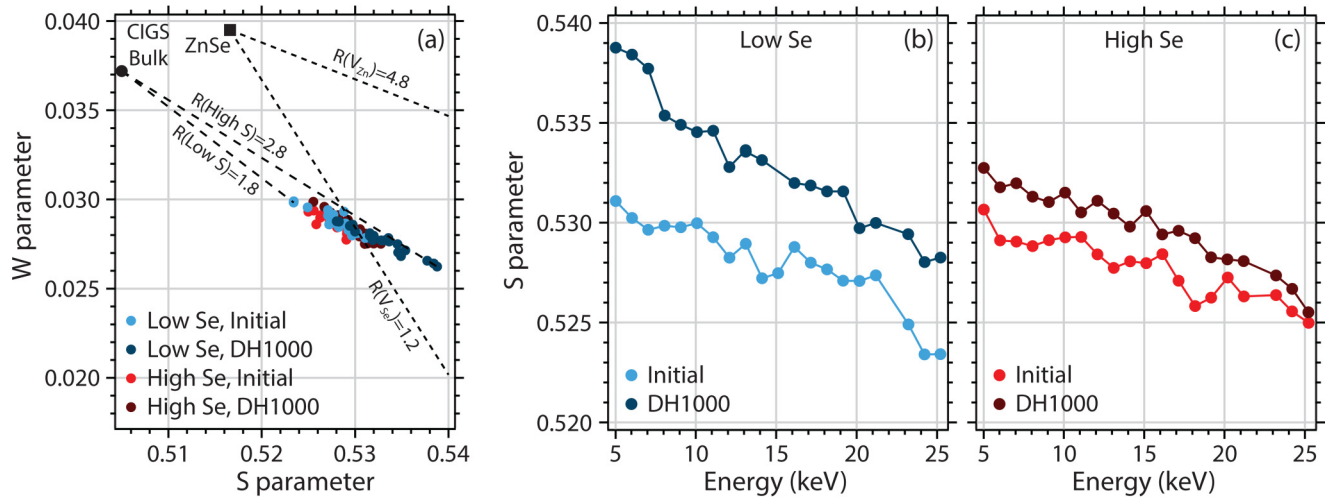


FIG. 4. The impact of dark-heat exposure (DH1000) on (a) the (S , W) parameters and (b) and (c) S parameter plotted against positron implantation energy (5–25 keV) for low and high pre-selenization samples. The energy range of 5–25 keV corresponds to a mean implantation depth range of 0.1–1.2 μm according to Ref. 28.

samples in this study. The dashed lines connecting the CIGS data points from our samples to the reference CIGS bulk crystal value indicate a range of R values spanning from $R = 1.8$ (for the lowest S value) to $R = 2.8$ (for the highest S value). Similar to observations for CGS and CIS samples, the values of R observed here for ACIGS are between $R(V_{Zn}) = 4.8$ for cation vacancies and $R(V_{Se}) = 1.2$ for anion vacancies in ZnSe , which is structurally very similar to CIGS.^{27,28} As suggested previously, this indicates a vacancy defect in ACIGS with a mixed nature of both cation and anion vacancies, pointing to the $V_{Se}-V_{Cu}$ divacancy as the dominant defect responsible for positron trapping in these samples.

The S parameter increases from the initial to DH1000 state for both “high” and “low” pre-selenization conditions, indicating that additional $V_{Se}-V_{Cu}$ divacancies are created with dark heat exposure. Additionally, the increase for the low pre-selenization sample is dramatically larger than for the high pre-selenization, suggesting that the Se deficiency results in the generation of more divacancies with dark heat. This can be seen more clearly in Figs. 4(b) and 4(c), where the S parameters are plotted as a function of positron implantation energy over the range of 5–25 keV. The divacancy concentrations increase with dark heat, with the effect being even more significant for the low pre-selenization sample, over the probed thickness of the absorber ($\sim 1.2\ \mu\text{m}$). A recent study of the effects of stress-induced changes in CIGS photovoltaic devices suggests that DH1000 treatment results in a reduction in the Na content within the absorber,²⁹ which could lead to depassivation of $V_{Se}-V_{Cu}$ divacancy complex donors (i.e., an increase in their density), consistent with early observations of the influence of Na from a thin NaF layer deposited prior to the CIGS absorber.³⁰ In addition, the $V_{Se}-V_{Cu}$ divacancy defect density is larger near the front interface of the absorber, when the positron implantation energy is the lowest. It should be noted that we have removed from the plots the data from below 5 keV where the back-diffusion of positrons to the surface dominates the data, and the shown depth

evolution are characteristic of the layer. This aspect is further investigated in Sec. II D using depth-dependent minority carrier lifetime measurements. In Sec. II E, we show that divacancy complexes can be electron traps and might be related to traps identified in TRPL analysis.^{31–33}

Next, we consider the photoluminescence properties of defect states identified with DLOS and PAS. Detection of PL is typically only possible for shallow defects, which can have sufficient radiative efficiency. Neither $E_v + 0.56\ \text{eV}$ nor $E_v + 0.98\ \text{eV}$ defects have PL emission signatures. To partially overcome this limitation, we employ TRPL excitation spectroscopy, which uses tunable optical excitation to directly excite defect states within the bandgap. After electron detrapping to the conduction band, we measure bandgap PL emission to record the “ $E_v + 0.98\ \text{eV}$ defect” absorption spectrum.³⁴

Figure 5 shows PL excitation spectra for the “low Se” and “high Se” ACIGS samples. This defect band is located close to the energy observed in Ref. 34 for a CIGS absorber material with a slightly lower bandgap ($E_g \approx 1.11\ \text{eV}$), suggesting that the chemical nature of the defect is similar. For the CIGS absorber in Ref. 34, we attributed this defect to the $V_{Se}-V_{Cu}$ divacancy complex based on first-principles calculations for the defect density of states. The experimental evidence from PAS, Fig. 3, qualitatively supports this assignment for the ACIGS absorber studied in this paper. We observe an increase in the intensity of the defect excitation peak after dark-heat exposure (DH1000), which indicates higher $V_{Se}-V_{Cu}$ divacancy density after stressing, consistent with the increase in the S parameter in the PAS data.

C. Depth-dependent carrier dynamics

Interface and bulk defects can have different impact on recombination losses. PAS data in Fig. 4(b) indicate depth-dependent $V_{Se}-V_{Cu}$ divacancy density, and in this section, we investigate

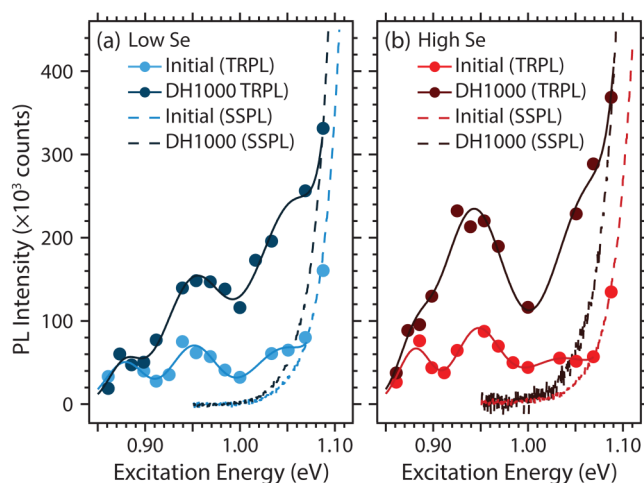


FIG. 5. The impact of dark-heat exposure (DH1000) on the sub-bandgap PL excitation spectra for the (a) low Se and (b) high Se ACIGS samples. The symbols are data extracted from the TRPL data following sub-bandgap excitation. The dashed lines are the low-energy tails of the steady-state PL spectrum, following excitation at 632.8 nm. The solid lines are a guide to the eye, to highlight the broad sub-bandgap defect absorption between 0.85 and 1.08 eV.

depth-dependent carrier lifetimes from variable-excitation-wavelength TRPL.

While the impact of silver alloying on the optical bandgap of ACIGS has been published,^{5,35} to our knowledge, the wavelength-dependent absorption coefficients for ACIGS absorbers are not well-known. For $\text{Ag}/(\text{Ag} + \text{Cu}) < 0.2$, the bandgap is quite close to the equivalent Cu-only material,³⁵ allowing us to use the established absorption coefficients for CIGS³⁶ to estimate that above bandgap excitation at 450 nm and 640 nm results in carrier generation within approximately 50 nm and 250 nm of the front interface, respectively. In contrast, sub-bandgap excitation (where the estimated absorption coefficient is >1000 times smaller) results in near-uniform carrier generation throughout the entire $1.2\ \mu\text{m}$ thickness of the ACIGS absorber. Within the framework of defect-mediated TRPL decay times described above, the ability to manipulate the carrier generation profile by varying the excitation wavelength allows us to probe the depth-dependent defect/trap distribution within the absorber layer.

Figures 6(a) and 6(b) show representative TRPL decays for excitation at 450 nm, 640 nm, 1180 nm, and 1260 nm for the “low Se” ACIGS samples, illustrating the impact of different carrier generation depths and DH1000 exposure. For above-bandgap excitation (450 nm and 640 nm), there is a distinct short decay component that we attribute either to carrier capture in traps or carrier redistribution within the absorber layer, similar to previous studies for CIGS.³⁷ In contrast, as shown in Fig. 5 (*vide supra*), sub-bandgap excitation (1180 nm or 1260 nm) results in direct population of the defect states close to the conduction band. This, coupled with the more uniform excitation profile, explains the absence of a fast decay component for this measurement condition. An exponential decay model was assumed for the slow time

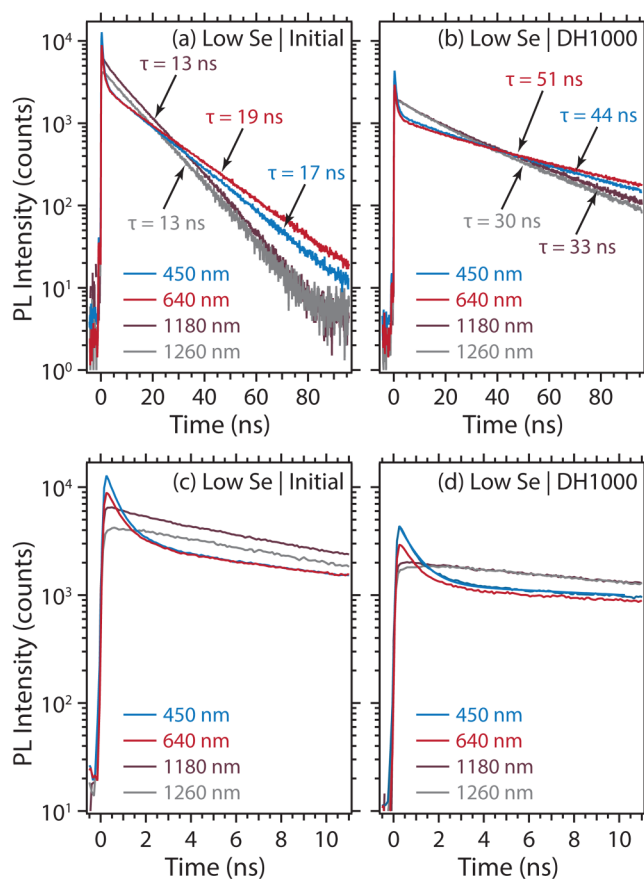


FIG. 6. Excitation wavelength-dependent TRPL decays for (a) initial and (b) DH1000-exposed ACIGS absorbers for the low pre-selenization condition, along with the PL lifetimes extracted from single-exponential fits. (c) and (d) represent the same data as (a) and (b) in the first 10 ns.

component, and the TRPL decay times that correspond to indicated measurement conditions are shown in Figs. 6(a) and 6(b). Before DH1000 exposure, decay times range from 13 ns (sub-bandgap excitation at 1180 nm or 1260 nm) to 19 ns (640 nm). After DH1000, the measured TRPL decay times increase by a factor of ca. 2.5, for both sub-bandgap excitation and above-bandgap excitation. For the “high Se” ACIGS sample before DH1000 exposure, the TRPL decay times range from ca. 13 ns (sub-bandgap excitation at 1180 nm or 1260 nm) to 16 ns (640 nm). After DH1000, the bulk sub-bandgap excitation decay time stays in the same range, 14–15 ns. In contrast, much larger changes are observed for 450 nm (59 ns) and 640 nm (64 ns) excitation. As we show in Sec. II E, this increase in TRPL decay times after dark heat treatment can be attributed to minority carrier (electron) trapping and/or a reduced SRH defect density. Depth-dependent TRPL decay times (Fig. S4 in the supplementary material) indicate that, in high-Se absorbers, the impact of dark heat predominantly occurs near the front interface.

As summarized above measurements for “low Se” absorbers indicate ca. 2.5 times increased TRPL lifetimes with DH1000, irrespective of the depth profile of the excitation. These observations suggest that minority carrier traps/recombination centers are distributed throughout the absorber, consistent with the $V_{\text{Se}}-V_{\text{Cu}}$ divacancy density directly measured with PAS (Fig. 4). In contrast, DH1000 has little impact on the measured sub-bandgap excitation lifetimes of the “high Se” in the bulk of the absorber layer, whereas the lifetimes for excitation at the front interface increase by a factor of ca. 4. This observation is consistent with a lower bulk density of defects related to selenium vacancies, since the high-Se absorbers are fabricated with additional selenization near the back contact (as described in Sec. II A).

D. Discussion of carrier dynamics

Here, we concentrate on the “low Se” sample, primarily because observed changes in device performance are larger for this sample. Assuming that the radiative recombination coefficient, B , of ACIGS is similar to that for CIGS (ca. $1.67 \times 10^{-10} \text{ cm}^3 \text{ s}^{-1}$),^{38,39} and a net acceptor concentration (determined by fast C-V), $N_A = 2 \times 10^{15} \text{ cm}^{-3}$ (Initial) and $1 \times 10^{15} \text{ cm}^{-3}$ (DH1000), we estimate radiative lifetimes, $\tau_{\text{rad}} = 1/(B \times N_A) = 3.0 \mu\text{s}$ (Initial) and $6.0 \mu\text{s}$ (DH1000). This radiative lifetime decreases to $>100 \text{ ns}$ for the light-soaked samples, where $N_A \approx 4-6 \times 10^{15} \text{ cm}^{-3}$. These lifetimes exceed the measured TRPL decay times, suggesting that the carrier dynamics are determined by non-radiative decay processes.

In the simplest case, we assume that minority carrier trapping/detrapping plays no role in the observed decay kinetics, and that the long TRPL decay time can therefore be attributed to SRH recombination (i.e., $\tau_{\text{decay}} = \tau_{\text{SRH}}$). Under these circumstances, the SRH recombination times, τ_{SRH} , are ca. $15.4 \pm 3.3 \text{ ns}$ (Initial) and $40 \pm 10 \text{ ns}$ (DH1000). Using the range of published electron capture cross sections of CIGS ($1.0-50 \times 10^{-14} \text{ cm}^2$),^{31,37,40,41} we estimate the density of SRH recombination centers to be in the ranges ca. $(0.03-1.5) \times 10^{14} \text{ cm}^{-3}$ (Initial) and ca. $(0.01-0.6) \times 10^{14} \text{ cm}^{-3}$ (DH1000). The densities of midgap states extracted from DLTS measurements (Fig. 3) for these two samples lie closer to the upper limit of these ranges, which would be consistent with a smaller electron capture cross section at the recombination center. For samples exposed to simulated 1 sun irradiation for 24 h the TRPL decay time is reduced to ca. $5 \pm 0.5 \text{ ns}$ (Fig. S6; supplementary material), indicating a shorter SRH recombination time and consistent with an increase in the SRH recombination center density.

In contrast, more complex kinetic models have been developed that incorporate the effects of carrier trapping/detrapping processes at defect states close to the conduction band,^{32,33} including some that consider energetic and/or spatial distributions of defect states.^{37,41} These models suggest that the long decay time observed by TRPL can either be attributed to SRH recombination (as in the simple picture described above) or by the characteristic time for the SRH recombination process modified by electron capture and release from the defect states, $\tau_{\text{decay}} = (\tau_e/\tau_c) \times \tau_{\text{SRH}}$. In the latter case, the estimated carrier capture (τ_c) and emission (τ_e) times for the ca. 0.2 eV trap would be ca. $<0.4 \text{ ns}$ and 5.0 ns , respectively. When trapping is significant, the SRH recombination time would

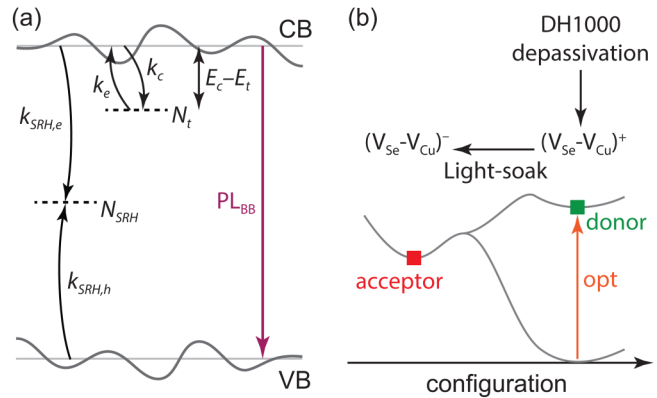


FIG. 7. (a) Kinetic scheme for photoinduced carrier dynamics in ACIGS absorbers, illustrating (1) capture (emission) of carriers to (from) a shallow defect near the conduction band, (2) SRH recombination via a deep, midgap defect state, and (3) band-to-band radiative carrier recombination. (b) Cartoon illustrating the effects of dark-heat (DH) treatment and light soaking (LS) on the equilibrium between metastable defect $V_{\text{Se}}-V_{\text{Cu}}$ divacancy configurations in ACIGS absorbers, adapted from Ref. 10. The orange arrow indicates optical excitation of the donor $V_{\text{Se}}-V_{\text{Cu}}$ divacancy defect configuration, which can interconvert to the acceptor $V_{\text{Se}}-V_{\text{Cu}}$ divacancy defect configuration.

be a factor of ca. >10 shorter than estimated above and, for the same range of electron capture cross sections at defect states within the bandgap, this would lead to an increase in the estimated SRH recombination center densities by a factor of >10 .

The observed changes in the TRPL decay kinetics are consistent with a modulation of the equilibrium between near-conduction band defects and deeper SRH recombination centers, via either dark-heat (DH1000) or light-soaking (LS24) treatments. While our current data do not allow us to conclusively connect our experimental observations to the $V_{\text{Se}}-V_{\text{Cu}}$ divacancy complex, our observations are consistent with the changes in the density of the $V_{\text{Se}}-V_{\text{Cu}}$ divacancies after DH1000 (cf. PAS data; Fig. 4) and the anticipated light-induced conversion of shallow defects into deeper defects predicted by the $V_{\text{Se}}-V_{\text{Cu}}$ optical cycle proposed by Lany and Zunger [Fig. 7(b)]. Future studies will focus on absorbers with better controlled density of the metastable divacancy centers and will explore the more complex defect state models.

Here, we note that the similar TRPL decay times for the Initial samples (Fig. S4 in the supplementary material) are consistent with similar SRH recombination and trap densities in the “high Se” and “low Se” samples. However, the insensitivity of sub-bandgap excitation lifetimes of the “High Se” sample to DH1000 suggests that the additional Se at the back contact prevents or reduces the extent of donor defect depassivation in the bulk. In contrast, the much longer lifetimes for the above-bandgap excitation after DH1000 suggest that the dark heat treatment has a much greater impact on the near-surface defect properties for high pre-selenization conditions. These observations suggest that control over the pre-selenization conditions and Na content provides a material processing strategy to control $V_{\text{Se}}-V_{\text{Cu}}$ divacancy defects and trap densities in ACIGS and related absorbers.

IV. CONCLUSIONS

We investigated the impact of metastable defects on the electro-optical properties of polycrystalline (Ag,Cu)(In,Ga)Se₂ (ACIGS) absorbers and devices. Through changes in the pre-selenization levels of the back electrode layer, we are able to determine that the dominant defects in the ACIGS absorber are associated with the metastable V_{Se}-V_{Cu} divacancy complex. Exposure of the samples to dark-heat (DH1000) appears to result in depassivation of these V_{Se}-V_{Cu} divacancies, resulting in an increase of the defect density measured by positron annihilation spectroscopy. The DH1000 treatment also causes an increase in near-conduction band defects, as determined by deep-level optical and time-resolved photoluminescence excitation spectroscopy, along with a decrease in the net acceptor concentration and density of midgap SRH recombination centers, as determined by deep-level transient spectroscopy. These changes in defect traps and recombination centers manifest themselves as an increase in the observed time-resolved photoluminescence decay time. Light-soaking under simulated 1 sun AM1.5G illumination for 24 h results in an increase in the doping density and associated reduction in the width of the depletion region. These effects manifest themselves as a reduction in the spectral response and short-circuit current density of the devices. This is particularly evident for the low pre-selenization condition, whereas the effects in the high pre-selenization sample are less pronounced. These results point to careful control of the selenization conditions as a method to manipulate the V_{Se}-V_{Cu} divacancy density and the resulting electro-optical properties and device performance.

SUPPLEMENTARY MATERIAL

See the [supplementary material](#) for the impact of the selenization level on the electronic bandgap, the impact of environmental stress on the spectral response of the photovoltaic devices, and a summary of the time-resolved photoluminescence decay lifetimes.

ACKNOWLEDGMENTS

This work was authored in part by the National Renewable Energy Laboratory, operated by Alliance for Sustainable Energy, LLC, for the U.S. Department of Energy (DOE) under Contract No. DE-AC36-08GO28308. A.J.F., P.D., and D.K. acknowledge funding provided by the U.S. Department of Energy Office of Energy Efficiency and Renewable Energy Solar Energy Technologies Office (SETO) Agreement No. 30306. P.K.P. and A.R.A. acknowledge funding from the U.S. Department of Energy (Contract No. DE-DD0007141). A.K. and F.T. acknowledge funding from the Academy of Finland under Project No. 315082 for positron annihilation spectroscopy measurements. The views expressed in the article do not necessarily represent the views of the DOE or the U.S. Government.

REFERENCES

- ¹M. A. Green, E. D. Dunlop, D. H. Levi, J. H. Ebinger, M. Yoshita, and A. W. Y. Ho Baillie, *Prog. Photovolt. Res. Appl.* **27**, 565 (2019).
- ²J. H. Boyle, B. E. McCandless, G. M. Hanket, and W. N. Shafarman, *Thin Solid Films* **519**, 7292 (2011).

- ³I. V. Bodnar, I. A. Viktorov, and S. L. Sergeev-Nekrasov, *Cryst. Res. Technol.* **33**, 885 (1998).
- ⁴P. T. Erslev, J. Lee, G. M. Hanket, W. N. Shafarman, and J. David Cohen, *Thin Solid Films* **519**, 7296 (2011).
- ⁵M. Edoff, T. Jarmar, N. S. Nilsson, E. Wallin, D. Högström, O. Stolt, O. Lundberg, W. Shafarman, and L. Stolt, *IEEE J. Photovolt.* **7**, 1789 (2017).
- ⁶M. Richards, in *MiaSolé In the News* (MiaSolé, A Hanergy Company, 2019), see <http://miasole.com/miasole-achieves-flexible-substrate-thin-film-solar-cell-efficiency-of-20-56-percent/>.
- ⁷M. Richards, in *MiaSolé In the News* (MiaSolé, A Hanergy Company, 2019), see <http://miasole.com/miasole-breaks-world-record-again-large-area-flexible-photovoltaic-module-with-18-64-efficiency/>.
- ⁸S. Siebentritt, M. Igalson, C. Persson, and S. Lany, *Prog. Photovolt. Res. Appl.* **18**, 390 (2010).
- ⁹D. Abou-Ras, S. Wagner, B. J. Stanbery, H.-W. Schock, R. Scheer, L. Stolt, S. Siebentritt, D. Lincot, C. Eberspacher, K. Kushiya, and A. N. Tiwari, *Thin Solid Films* **633**, 2(2017).
- ¹⁰S. Lany and A. Zunger, *J. Appl. Phys.* **100**, 113725 (2006).
- ¹¹M. Igalson, M. Cwil, and M. Edoff, *Thin Solid Films* **515**, 6142 (2007).
- ¹²M. Igalson, M. Maciaszek, K. Macielak, A. Czudek, M. Edoff, and N. Barreau, *Thin Solid Films* **669**, 600 (2019).
- ¹³J. Bailey, G. Zapalac, and D. Poplavskyy, in *Proceedings of the 2016 IEEE 43rd Photovoltaic Specialists Conference (PVSC)*, Portland, OR, USA, 5–10 June 2016, IEEE, 2016, p. 2135.
- ¹⁴R. Farshchi, B. Hickey, G. Zapalac, J. Bailey, D. Spaulding, and D. Poplavskyy, in *Proceedings of the 2016 IEEE 43rd Photovoltaic Specialists Conference (PVSC)*, Portland, OR, USA, 5–10 June 2016, IEEE, 2016, p. 2157.
- ¹⁵P. Blood and J. W. Orton, *The Electrical Characterization of Semiconductors Majority Carriers and Electron States* (Academic Press, San Diego, CA, 1992).
- ¹⁶P. K. Paul, K. Aryal, S. Marsillac, S. A. Ringel, and A. R. Arehart, in *Proceedings of the 2016 IEEE 43rd Photovoltaic Specialists Conference (PVSC)*, Portland, OR, USA, 5–10 June 2016, IEEE, 2016, p. 2246.
- ¹⁷P. K. Paul, K. Aryal, S. Marsillac, T. J. Grassman, S. A. Ringel, and A. R. Arehart, in *Proceedings of the 2016 IEEE 43rd Photovoltaic Specialists Conference (PVSC)*, Portland, OR, USA, 5–10 June 2016, IEEE, 2016, p. 3641.
- ¹⁸E. Farzana, M. F. Chaiken, T. E. Blue, A. R. Arehart, and S. A. Ringel, *APL Mater.* **7**, 022502 (2018).
- ¹⁹F. Tuomisto and I. Makkonen, *Rev. Mod. Phys.* **85**, 1583 (2013).
- ²⁰B. Hickey, H. Loi, and R. Farshchi, in *Proceedings of the 2018 IEEE 7th World Conference on Photovoltaic Energy Conversion (WCPEC)*, Waikoloa Village, HI, USA, 10–15 June 2018, IEEE, 2018, p. 0131.
- ²¹R. Farshchi and D. Poplavskyy, in *Proceedings of the 2018 IEEE 7th World Conference on Photovoltaic Energy Conversion (WCPEC)*, Waikoloa Village, HI, USA, 10–15 June 2018, IEEE, 2018, p. 2616.
- ²²S. Chen, T. Jarmar, S. Södergren, U. Malm, E. Wallin, O. Lundberg, S. Jander, R. Hunger, and L. Stolt, *Thin Solid Films* **582**, 35 (2015).
- ²³P. K. Paul, T. Jarmar, L. Stolt, A. Rockett, and A. R. Arehart, *arXiv: 1806.06665* (2018).
- ²⁴S.-H. Wei, S. B. Zhang, and A. Zunger, *Appl. Phys. Lett.* **72**, 3199 (1998).
- ²⁵P. K. Paul, D. W. Cardwell, C. M. Jackson, K. Galiano, K. Aryal, J. P. Pelz, S. Marsillac, S. A. Ringel, T. J. Grassman, and A. R. Arehart, *IEEE J. Photovolt.* **5**, 1482 (2015).
- ²⁶J. I. Deitz, P. K. Paul, R. Farshchi, D. Poplavskyy, J. Bailey, A. R. Arehart, D. W. McComb, and T. J. Grassman, *Adv. Energy Mater.* **9**, 1901612 (2019).
- ²⁷K. Saarinen, T. Laine, K. Skog, J. Mäkinen, P. Hautojärvi, K. Rakennus, P. Uusimaa, A. Salokatve, and M. Pessa, *Phys. Rev. Lett.* **77**, 3407 (1996).
- ²⁸E. Korhonen, K. Kuitunen, F. Tuomisto, A. Urbaniak, M. Igalson, J. Larsen, L. Gütay, S. Siebentritt, and Y. Tamm, *Phys. Rev. B* **86**, 064102 (2012).
- ²⁹R. Farshchi, B. Hickey, and D. Poplavskyy, in *Proceedings of the 2017 IEEE 44th Photovoltaic Specialists Conference (PVSC)*, Washington, D.C., USA, 25–30 June 2017, IEEE, 2017.

- ³⁰M. A. Contreras, B. Egaas, P. Dippo, J. Webb, J. Granata, K. Ramanathan, S. Asher, A. Swartzlander, and R. Noufi, in *Proceedings of the 1997 IEEE 26th Photovoltaic Specialists Conference (PVSC)*, Anaheim, CA, USA, 29 Sept.-3 Oct. 1997, IEEE, 1997), p. 359.
- ³¹M. Maiberg, T. Hölscher, S. Zahedi-Azad, and R. Scheer, *J. Appl. Phys.* **118**, 105701 (2015).
- ³²M. Maiberg, T. Hölscher, S. Zahedi-Azad, W. Fränzel, and R. Scheer, *Appl. Phys. Lett.* **107**, 122104 (2015).
- ³³M. Maiberg, T. Hölscher, E. Jarzembowski, S. Hartnauer, S. Zahedi-Azad, W. Fränzel, and R. Scheer, *Thin Solid Films* **633**, 208 (2017).
- ³⁴S. A. Jensen, A. Kanevce, L. M. Mansfield, S. Glynn, S. Lany, and D. Kuciauskas, *Sci. Rep.* **7**, 13788 (2017).
- ³⁵J. H. Boyle, B. E. McCandless, W. N. Shafarman, and R. W. Birkmire, *J. Appl. Phys.* **115**, 223504 (2014).
- ³⁶M. I. Alonso, M. Garriga, C. A. Durante Rincón, E. Hernández, and M. León, *Appl. Phys. A* **74**, 659 (2002).
- ³⁷S. J. Heise, V. Gerliz, M. S. Hammer, J. Ohland, J. Keller, and I. Hammer-Riedel, *Sol. Energy Mater. Sol. Cells* **163**, 270 (2017).
- ³⁸M. Maiberg and R. Scheer, *J. Appl. Phys.* **116**, 123710 (2014).
- ³⁹T. P. Weiss, B. Bissig, T. Feurer, R. Carron, S. Buecheler, and A. N. Tiwari, *Sci. Rep.* **9**, 5385 (2019).
- ⁴⁰M. Gloeckler, A. L. Fahrenbruch, and J. R. Sites, in *Proceedings of the 2003 IEEE 3rd World Conference on Photovoltaic Energy Conversion (WCPEC)*, Osaka, Japan, 11–18 May 2003, IEEE, 2003), p. 491. <http://ieeexplore.ieee.org/document/1305328>.
- ⁴¹J. F. López Salas, S. J. Heise, M. Richter, V. Gerliz, M. S. Hammer, J. Ohland, and I. Hammer-Riedel, *Thin Solid Films* **633**, 40 (2017).